JOURNAL OF OPTOELECTRONICS AND ADVANCED MATERIALS Vol. 13, No. 11-12, November – December 2011, p. 1542 - 1547

Size dependence of melting process of ZnSe nanowires: molecular dynamics simulations

S. SENGUL, S. SENTURK DALGIC*
Department of Physics, Faculty of Science, University of Trakya, 22030, Edirne – Turkey

It is known that the stable crystal structure of ZnSe nanowires depends on the nanowire diameter. For this reason, we have focused on the impact of size of ZnSe nanowires on their structural properties. The molecular dynamics (MD) simulations have performed to especially discuss consequences for size effect on melting process for ZnSe nanostructures with cylindrical shape. The interactions between the atoms in system have defined by an empirical model potential developed for semiconductor metal-chalcogenides. The nanowires studied in this work have a different number of diameters and have generated by assembling the zincblende unit cell. Periodic boundary conditions have applied only along c- axis. The size effect on melting of nanowires has investigated. Some structural and dynamic properties such as distribution functions, mean square displacements and diffusion coefficients have also calculated to get detailed information about the nature of melting process of ZnSe nanowires. Calculations show that melting temperatures of ZnSe nanowires are lower than that of bulk and highly related with the size of the nanowires.

(Received June 2, 2011; accepted November 23, 2011)

Keywords: ZnSe nanowires, Tersoff potentials, Molecular dynamics simulations

1. Introduction

One-dimensional (1D) nanostructures, nanowires have attracted a great deal of research interest in recent years, because of their importance in fundamental low-dimensional physics research as well as in technological application. Among these 1D nanostructures, semiconductor nanowires (NWs) including groups II-VI semiconductors are promising candidates for applications in nanoscale electronic and optoelectronic devices [1] and have various potential applications in both theoretical and applied research areas [2] in the context of their highly size and shape-dependent properties. As one of the typical II–VI semiconductors, ZnSe is a tetrahedrally bonded IIB-VIA semiconductor compound with zinc-blende structure having large band gap of 2.68 eV and has perfect optical properties as well as good electrical properties. These features make ZnSe a kind of well-known luminous, laser material and have a wide application in the fabrication of blue–green light-emitting diodes, nonlinear optical-electronic components, dielectric mirrors and infrared devices [3-7].

Generally, the semiconductor materials of II-VI have the cubic zinc blende (ZB) and hexagonal wurtzite (WZ) structures. For most II-VI semiconductors such as ZnS, ZnSe, and CdTe, the bulk ZB structure is energetically more favorable than that of the WZ one [8, 9]. Authors have argued a comprehensive understanding of the phase transition of II-VI semiconductor nanocrystals by an analytical thermodynamic model based on the first principles calculations. It has noted that the WZ phase become thermodynamically stable as the size of nanocrystals decreases for ZnS, ZnSe, ZnTe, and CdTe, and the phase transition size is temperature-dependent. ZnSe systems studied in this work have been considered in ZB phase, which belongs to F-43 m space group, and there are four Zn atoms around every Se atom. In comparison with wurtzite structure very little is known about the electronic, optical and mechanical properties of ZB II–VI groups under higher pressure and temperature. Benkabou et.al. have determined an empirical interatomic potential parameters for this group of semiconductors and calculated structural properties of bulk ZnSe by microscopic simulations in order to understand the nature of ZB structure in high temperature [10]. They have found a good agreement between the calculated and experimental values for ground state, elastic and thermal properties in the temperature range of 0 to 1000 K. These temperatures are too lower from melting temperature of ZnSe which is the value of 1795 K [11,12]. In thermodynamic point of view, nanomaterials are treated as metastable materials, and thermal stability of nanomaterials is very important for their applications [13]. When the dimensions of system reduce to nanoscale, surface – volume ratio becomes very larger, which leads to decrease of melting temperature, and the nanomaterials exhibit different thermodynamic properties result from the size effect of materials.

The purpose of the present work is to employ the Tersoff potential in conjunction with the molecular simulation method to investigate the structural evolution and dynamics associated with the size dependence of melting temperature of ZnSe NWs.

2. Method of calculation

The prior condition for the success of MD calculation is the availability of reliable interatomic potentials

describing the interaction between atoms in the crystalline lattice. In the present MD simulation, the lattice of a crystal was built from particles interacting via three-body potentials by means of the empirical bond order potential proposed by Tersoff [14]. The interatomic potential energy is then the sum of repulsive and attractive parts of the potential. Tersoff potential between two neighboring atoms *i* and *j* can be formally written as a summation of pair-wise interactions,

$$V_{ij} = f_c(r_{ij})\left[f_R(r_{ij}) - b_{ij} f_A(r_{ij})\right] \tag{1}$$

where r_{ij} is length of the *ij* bond, $f_R(r_{ij})$ denotes the repulsive part of the potential, such as the core-core interactions. The function $f_A(r_{ij})$ represents the bonding due to the valence electrons, The $f_C(r_{ij})$ is the cutoff function which explicitly restricts the interactions within the nearest neighbors and dramatically reduces the redundant computation in the force potential evaluation procedure, and their functional forms are given as

$$f_R(r_{ij}) = A_{ij}\exp(-\lambda_1 r_{ij}),\ f_A(r_{ij}) = B_{ij}\exp(-\lambda_2 r_{ij}), \tag{2}$$

$$f_C(r_{ij}) = \begin{cases} 1, & r_{ij} < R_{ij} \\ \frac{1}{2}\left[1 + \cos[\pi(r_{ij} - R_{ij})/(S_{ij} - R_{ij})\right], & R_{ij} \le r_{ij} \le S_{ij} \\ 0, & r_{ij} > S_{ij} \end{cases} \tag{3}$$

where b_{ij} is a bond order parameter defining how the bond-formation energy is affected by local atomic arrangement around atoms *i* and *j*. The functional form of b_{ij} can be written as:

$$b_{ij} = (1 + (\beta\xi_{ij})^{n_i})^{-1/2n_i} \tag{4}$$

with

$$\xi_{ij} = \sum_{k\neq i,j} f_C(r_{ij})\, g(\theta_{ijk}) \exp(\lambda_3^3 (r_{ij} - r_{ik})^3) \tag{5}$$

$$g(\theta_{ijk}) = 1 + \frac{c^2}{d^2} - \frac{c^2}{d^2 + (h - \cos(\theta_{ijk}))^2} \tag{6}$$

where ξ_{ij} is the effective coordination number and $g(\theta_{ijk})$ is a function of the angle between r_{ij} and r_{ik}. All these potential parameters have been given in Ref.[10].

The MD simulations in this work are performed with the DL-POLY software package [15]. In our calculations for the bulk ZnSe and NWs, we used the same parameters given by Benkabou et.al. to describe the atomic interactions [10]. This potential successfully reproduces the ZnSe single crystalline lattice parameters. It is followed as two styles of dynamics: *i)* In order to get an energy-optimized structure during heating at a given temperature for the bulk system of 512 ions (Zn:256, Se:256), the standard constant number of particles, pressure and temperature (NPT) MD calculations were performed with a periodic boundary conditions. *ii)* the NWs, however, were simulated at ensemble of the constant number of particles, volume and temperature (NVT). We formed seven NWs as a cylindrical shape with diameters varying from 2nm to 8nm to investigate the melting processes of NWs. ZnSe NWs were constructed from a large cubic ZB crystal using various cylindrical cutoff radii. In the crystallographic [100] and [010] directions, the ZnSe NWs were constructed a finite number of unit cells, while in the [001] direction an infinite wire was obtained by applying the periodic boundary conditions. At as a first step, both bulk and nanowire have been stabilized by relaxing for 100ps at 300 K given conditions. Then, the heating process was simulated by the temperature increment of ΔT=100K. However, the temperature increases were around of ΔT=10K near the melting region. The simulations were carried out for 100ps (60ps relaxation + 40ps calculation) at each temperature. The Newtonian equations of motion are integrated using the Leapfrog Verlet method with a time step of 1.0 fs. The desired temperature and ambient pressure were controlled by Nose-Hoover thermostat [16, 17].

The pair distribution function g(r) is regarded as one of the most important parameters that is used to describe the structure characterization of solid, amorphous and liquid states as

$$g(r) = \frac{\Omega}{N^2}\left\langle \left(\sum_{i=1}^{N_i} n_i\right) / 4\pi r^2 \Delta r \right\rangle \tag{7}$$

where, $g(r)$ is the probability of finding an atom in a distance ranging from r to $r+\Delta r$. Ω is simulated volume of unit cell. N is the Number of atoms in the systems, and N_i is the averaged number atom around *i*th atoms sphere shell ranging r to $r+\Delta r$, where Δr is the step of calculation. The diffusion coefficients of the atoms was calculated by using the Einstein equation

$$D = \lim_{t\to\infty} \frac{\left\langle \Delta r(t)^2 \right\rangle}{6t} \tag{8}$$

where t is the diffusion time, $\left\langle \Delta r(t)^2 \right\rangle$ is the mean square displacement (MSD). MSD of the particle in the MD simulations is assured by

$$\left\langle \Delta r(t)^2 \right\rangle = \frac{1}{N}\sum_{i=1}^{N} \left| r_i(t + t_o) - r_i(t_o) \right|^2 \tag{9}$$

where $r_i(t_o)$ is the position vector of the *i*th particle for the system in its initial configuration and $r_i(t)$ is the position vector of *i*th particle at time t.

3. Results and discussion

In order to re-test a performance of potential model used and potential parameters in these simulations, we performed a series of relevant MD simulations. The

calculated ground state total energy as a function of lattice parameter is plotted in Fig. 1 for ZB ZnSe along with a non-linear fit. The equilibrium lattice parameter can be clearly seen from figure as 5.671 A for cubic ZB structure which is very close to experimental value of 5.667 A [18].

Fig. 2 shows the temperature dependence of total energy. It can be seen from Fig. 1 that total energy has sharp decreasing and increasing at the temperatures of 820 K and 1780 K, respectively, which means an appearance of phase transition solid to solid and melting of bulk ZnSe. The melting temperature obtained by simulation T_m = 1780 K is 15K lower than the experimental melting temperature value of 1795 K [11,12] for ZnSe. These results for lattice parameter and melting point of bulk ZnSe is another indicator that the Tersoff potential is suitable to study of melting point of ZnSe. Fig. 2 also shows the heat capacity C_P calculated by the definition $C_P = (dE/dT)_P$ at 300 K as a function of temperature. The C_P is 26.6 J/molK which is very close to the experimental value at room temperature of *3R* where *R* is universal gas constant. With the increase of temperature to 820 K, C_P has sudden decreasing. Around melting temperature, the C_P abruptly increases and begins to fluctuate around 100 J/molK. An abrupt increase of C_P is occurred at 1780K due to the melting transition. As the temperature is higher than 1950K, solid state of ZnSe is completely transformed to liquid ZnSe.

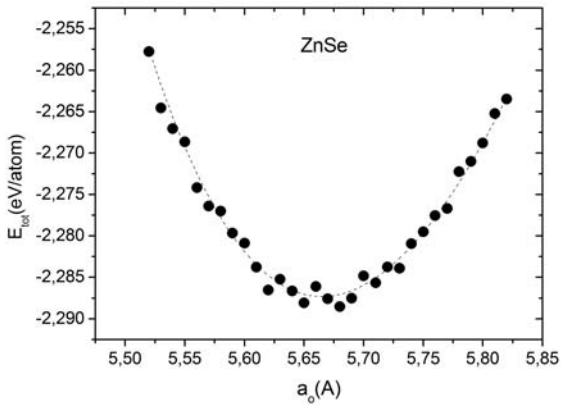

Fig. 1. The total energy of ZnO as a function of the lattice parameter in ZB structure.

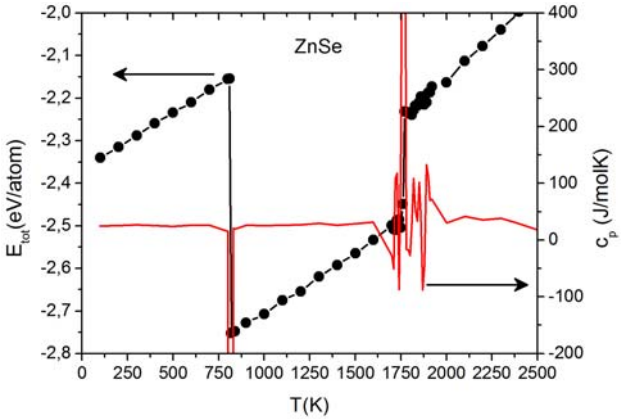

Fig. 2. Temperature dependence of the total energy and heat capacity for bulk ZnSe.

The pair distribution function, *g(r),* is one of the most important quantities to characterize structure of the system, especially for liquids. We have calculated pair distribution functions for bulk ZnSe in ZB structure at five different temperatures which correspond to critical points of energy-temperature curve. Fig. 3 shows the calculated *g(r)* functions compared with other simulated result taken from Ref. [10]. It can be seen that the *g(r)* calculated at 300K presents a good agreement with simulated ones and has a feature of solid structure. As the temperature increases, peaks of *g(r)* become wider. When the temperature reaches 820 K, it is occurred solid-solid phase transition in ZnSe. At this temperature the main peak position of *g(r)* slightly shifts to larger r values. There are various experimental studies such as Raman scattering and energy-dispersive X-ray diffraction which report the phase transitions between the ZB and rock salt (RS) structures under high pressure [19,20]. Because the main aim of this work is melting process, it will not discuss in detail the phase transition solid to solid. The g(r) of ZnSe shows an obvious first peak, visible second peak and featureless tail at 1780 K which corresponds to melting temperature obtained by MD simulations. It is noted that the absence of strong peaks in *g(r)s* at distance larger than the second peak position is typical for non-crystalline structure and crystalline structure loses its long range order and begins to melt.

For now, we can discuss results of MD simulations performed to study effect of the size (diameter) of NWs on melting points. It is remembered that simulation scheme of ZnSe NWs was similar to that of bulk ZnSe except that the NWs were simulated in NVT ensemble. Temperature dependence of total energies of these NWs are plotted in Fig. 4. Because of the surface energies, total energies of NWs are higher than that of bulk, and their energies closes to value of bulk as the diameter of NWs is reduced. Two transition regions are observed in the energy-temperature curves as shown in figure. The first distinction of the linearity is related with the solid - solid phase transition occurred the higher temperatures than room temperatures range within 300K – 450K. The second discontinuity is observed at relatively much higher temperatures. As diameter of NWs is increased, overall melting temperatures of NWs are increased and getting lower than that of bulk ZnSe. In Fig. 4, the total energy begins to deviate from linearity around the melting temperature, which means that the melting starts. The total energy reaches its maximum value at melting point, then decreases abruptly with the further increase of temperature (neck). The inset shows the behavior of total energy up close in Fig. 4. The breaking of ZnSe NWs and the formation of ZnSe spherical clusters is responsible of these abruptly decreasing. As the temperature increases, total energy has a linear relation with temperature that implies that the formed spherical clusters have not a split into smaller clusters. In our simulations, these necks disappear for the NWs with the diameters of 6.81nm and 8.02nm. The reason of this behavior is that the length of NWs in [001] direction is not large enough.

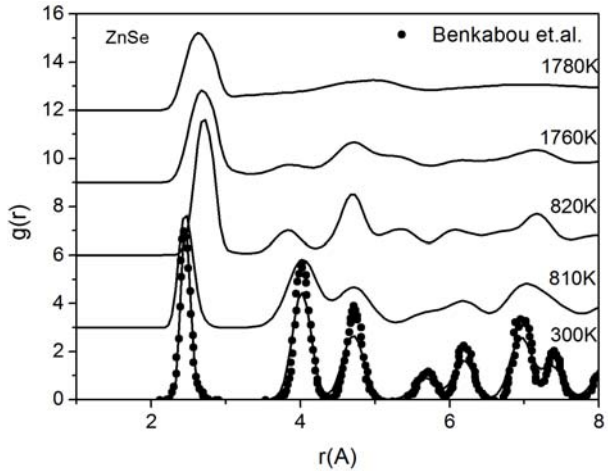

Fig. 3. Pair distribution functions calculated at different temperatures for bulk ZnSe.

In Fig. 5, we have displayed pair distribution functions for ZnSe NW with the diameter of 6.01nm along with the calculated ones for bulk ZnSe at different temperatures which correspond to critical points in energetic curve (Fig. 4). It can be done same comments for *g(r)s* of bulk and NW because the obvious difference between nanowires and their bulk counterparts is size. From figure, it can be recognized that the early solid – solid transition is occurred due to presence of the shifting peak positions of *g(r)*. As the temperature increasing to 1680K, which corresponds that ZnSe NW completely melts, the explicit first and visible second peaks of g(r) is formed. After melting, the behavior of *g(r)s* are almost same with bulk.

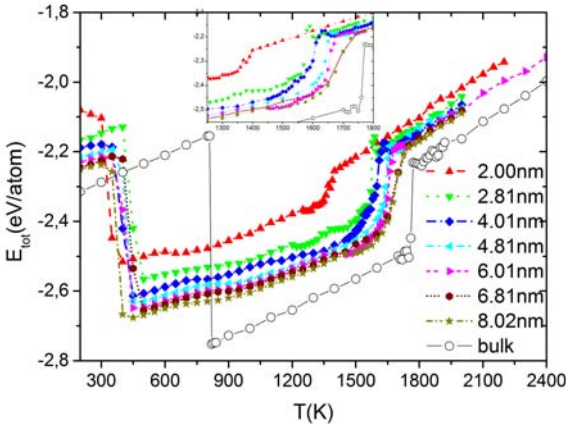

Fig. 4. Temperature dependence of the total energy of ZnSe NWs.

The temperature evaluations of diffusion coefficients for Zn atoms in different size of ZnSe nanowires have been plotted in the top of Fig. 6 along with an inset, which shows the structural transition at low temperature for Zn atoms. Because the diffusive behavior is commonly same, the results belong to Se atoms in ZnSe is not showed in this work. We have observed that the diffusion coefficients rapidly increase after melting temperature and the nanowire that has lowest melting temperature shows more diffusive behavior than that of nanowires has higher melting temperature. It can be seen that the all systems have reached same diffusion limit after melting temperature of bulk ones. There are some higher peaks in diffusion coefficients resulted from formation of ZnSe spherical clusters.

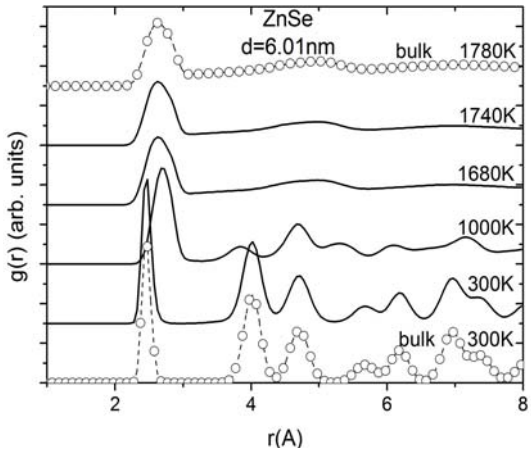

Fig. 5. Pair distribution functions calculated at different temperatures for ZnSe NW with the diameter of d=6.01nm.

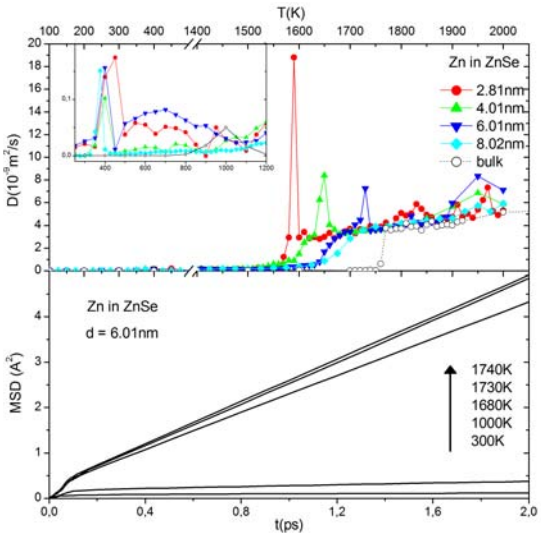

Fig. 6. Calculated diffusion coefficients (top) and mean square displacements (bottom) for Zn in ZnSe NWs.

In order to get detailed information of microscopic atomic motions, MSD functions have calculated by atomic trajectories deduced from molecular dynamics simulations. It is displayed only Zn atoms in ZnSe NWs with diameter of 6.01nm at the bottom part of Fig. 6. At lower temperatures, MSD has solid like behavior. As one goes through to higher temperature MSD changes its form solid like to liquid like.

In order to see the structure evolution process of ZnSe NWs, we display snapshots of trajectories of atomic motions at selected various temperatures and times for ZnSe NW with diameter of 6.01nm in Fig. 7. The first snapshot of figure shows NW at 300K constructed at the ZB structure. When the temperature increases up to

1000K, atoms placed into new lattice points and the system goes another solid phase. Up to 1680K, surface atoms of nanowires begin to deviate from their positions and a considerable disorder of surface regions is observed. Overall melting is reached at the temperature of 1680K. The neck was firstly formed in NW with diameter of 6.01nm at around 1680K and was relatively unstable during the relaxation. The breaking of NW can be seen in snapshot for the 1730K and the further relaxation performed leads to the formation of clusters as plotted in figure. The cluster resulted from applied periodic boundary condition in axial direction of NW is shown in final snapshot of Fig. 7 which correspond to higher jumping in diffusion coefficient (Fig. 6).

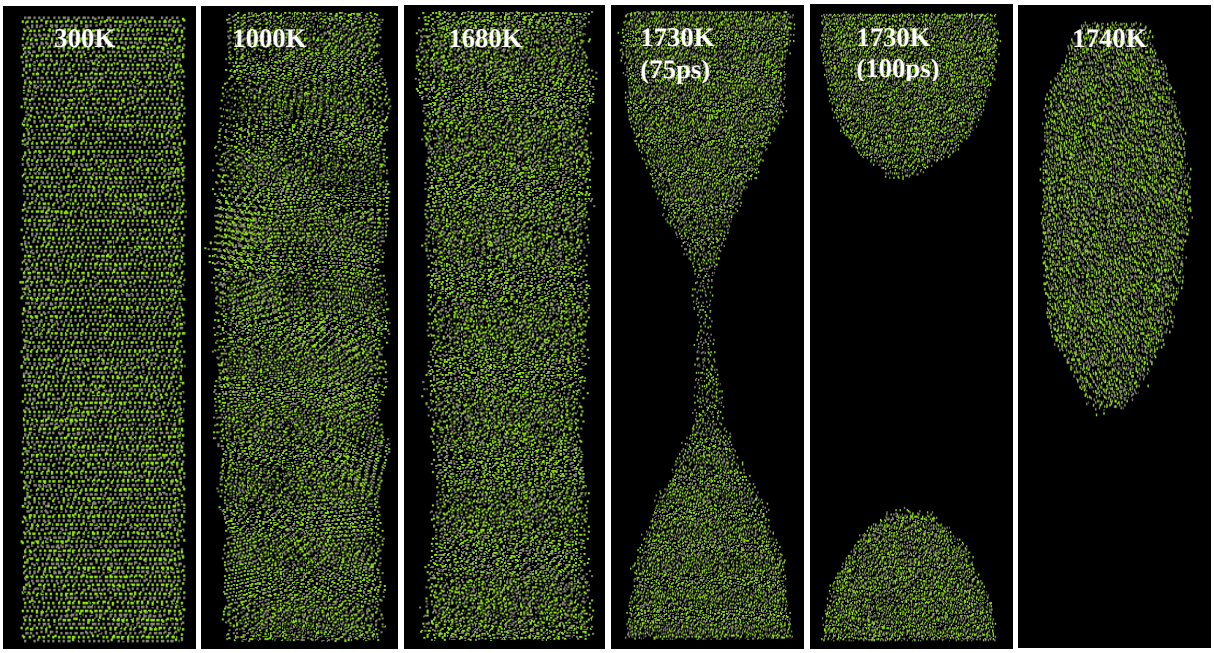

Fig. 7. Simulation snapshots of the ZnSe NW with the diameter of 6.01nm at different temperatures.

The size dependence of melting temperatures of ZnSe NWs is shown in Fig. 8. It is also included the results obtained from the theoretical model proposed by Li *et.al* [21]. Dashed line represents the melting point of bulk ZnSe in Fig. 8. As the mentioned, the melting point of ZnSe NWs increases with diameter. This result is in a good agreement with the prediction of thermodynamic model. The melting is a phase where the atomic bonds are broken. For the nanoscale, the ratio of surface atoms to volume atoms increases rapidly as the particle size decreases. As a result, surface energy increases and melting temperature decreases, pronouncedly.

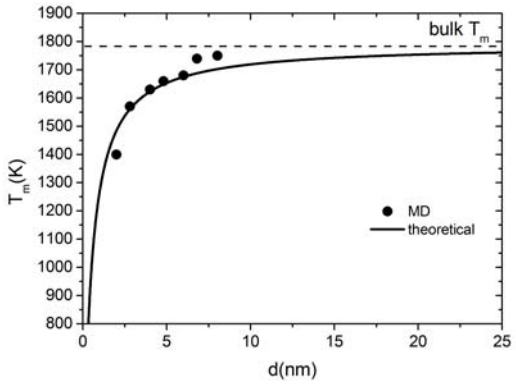

Fig. 8. The melting temperature as a function of diameter of ZnSe NWs.

4. Conclusions

In this paper, we have investigated the size effect on melting of ZnSe nanowires with cylindrical shape by the molecular dynamics simulations in which interactions defined by means of the empirical bond order potential proposed by Tersoff. We show that, melting temperatures of ZnSe nanowires are lower than that of bulk ZnSe and decreases with reducing diameter in nanoscale regime. When the nanowires were heated up above melting temperature, a neck of a nanowire began to arise and diameter of neck decreased rapidly with time. After the necks were arisen, breaking of nanowires lead to the formation of ZnSe clusters.

References

[1] R. Agarwal, C. M. Lieber, Appl. Phys. A **85**, 209 (2006)
[2] H. Mattousi, J. M. Mauro, E. R. Goldman, G. P. Anderson, V. C. Sundar, F. V. Mikulec, M. G. Bawendi, J. Am. Chem. Soc. **122**, 12142 (2000).
[3] D. B. Eason, Z. Yu, W. C. Hughes, W. H. Roland, C. Boney, J. W. Cook Jr., J. F. Schetzina, G. Cantwell, W. C. Harsch, Appl. Phys. Lett. **66**, 115 (1995).

[4] M. Godlewski, E. Guziewicz, K. Kooalko, E. Lusakowska, E. Dynowska, M. M. Godlewski, E. M. Godys, M. R. Phillips, J. Lumin. **102–103**, 455 (2003).
[5] H. R. Dobler, Appl. Opt. **28**, 2698 (1989).
[6] N. Sankar, K. Ramachandran, J. Crystal Growth **247**, 157 (2003)
[7] X. Wang, D. Huang, C. Sheng, G. Yu, J. of Appl. Phys. **90**, 6114 (2001).
[8] C. Ma, D. Moore, Y. Ding, J. Li, Wang, Z. L. Int. J. Nanotechnol. **1**, 431 (2004).
[9] S. Li, G. W. Yang J. Phys. Chem. C **114**, 15054 (2010).
[10] F. Benkabou, H. Aourag, M. Certier, Mat. Chem. Phys. **66**, 10 (2000)
[11] H. Okada, T. Kawanaka, S. Ohmoto, J. Crystal Growth **165**, 1 (1996)
[12] D. R. Lide (Ed.) Handbook of Chemistry and Physics, 80th. Ed.(CRC Publications, 1999-2000.
[13] A. S. Edelstein, R. C. Cammarata, Nanomaterials: Synthesis, Properties and Applications, Institute of Physics Publ., 1998.
[14] J. Tersoff, Phys. Rev. B **39**, 5566 (1989).
[15] DL_POLY: a molecular dynamics simulation package written by W. Smith, T.R. Forester and I.T. Todorov has been obtained from the website http://www.ccp5.ac.uk/DL_POLY
[16] S. Nose, J. Chem. Phys. **81**, 511 (1984).
[17] W. Hoover, Phys. Rev. A **31**, 1695 (1985).
[18] O. Madelung (Ed.), Landolt-Bornstein: New Series III, vol. 22, Springer, Berlin, 1987.
[19] A. K. Arora, T. Sakuntala, Phys. Rev. B **52**, 11052 (1995).
[20] C. M. Lin, D.S. Chuu, J. Appl. Phys. **101**, 103535 (2007).
[21] Y. J. Li, W. H. Qi, B. Y. Huang, M. P. Wang, S. Y. Xiong, Mod. Phys. Lett. B **24**, 2345 (2010).

*Corresponding author: serapd@trakya.edu.tr